J E M T
Journal of Earth and Marine Technology
homepage URL: ejurnal.itats.ac.id/jemt

Petrology and Geochemistry of Volcanic Rocks of Kaba Volcano, Bengkulu

Muhammad Eval Juni Wijaya *[1], Sakilla Gia Mentari[1], Ridho Ramadhan Pratama[1], Victor Ranson Sitohang[1]
[1] Department of Geology Engineering, Institut Teknologi Sumatera, Indonesia
*corresponding author e-mail: muhammad.wijaya@gl.itera.ac.id

Article info
Received: Jan 2, 2026
Revised: Feb 11, 2026
Accepted: Feb 12, 2026
Published: Apr 13, 2026

Keywords:
Petrology, Geochemistry, Volcanic Rocks, Kaba Volcano, Bengkulu.

Abstract

Mount Kaba is an active stratovolcano in Bengkulu Province, Indonesia, characterized by explosive magmatic eruptions and the presence of monogenetic volcanic centers, reflecting complex magmatic processes. This study focuses on the northern sector of the Mount Kaba area to investigate magma evolution and its relationship to volcanic development and hazard mitigation. Fifteen representative lava and pyroclastic rock samples were analyzed using petrographic observations and ICP-MS geochemical methods to determine major, trace, and rare earth element (REE) compositions. Petrographic results indicate basaltic to andesitic rocks with hypocrystalline textures, dominated by plagioclase, pyroxene, olivine, hornblende, and displaying porphyritic, trachytic, sieve, zoning, intersertal, and reaction rim textures that reflect disequilibrium processes and multi-stage magma evolution. Geochemically, rocks range from basanite/tephrite to dacite and belong mainly to calc-alkaline to high-K calc-alkaline magma affinities, forming two magma groups (Danau Mas and Kaba). Major element Harker diagrams show decreasing MgO, CaO, FeO, TiO_2 with increasing SiO_2 and increasing Na_2O + K_2O, indicating progressive differentiation. Trace element diagrams display positive trends of LILE and HFSE with SiO_2 and dual magma trends, suggesting multiple differentiation histories. Spider diagrams reveal LILE enrichment, HFSE depletion, and LREE enrichment relative to HREE, consistent with subduction-related magma sources. Integration of petrographic and geochemical data indicates that magma evolution was dominated by fractional crystallization, with additional influences from assimilation and magma mixing that produced compositional diversity and disequilibrium textures. Overall, the Mount Kaba magmatic system reflects a dynamic subduction zone environment characterized by multiple magma sources, progressive differentiation, and complex interactions within the crust, with implications for understanding volcanic processes and hazard potential in the northern sector.

1. Introduction

Mount Kaba is an active volcano located in the eastern part of Bengkulu Province, precisely in the Barisan Mountains [1]. The currently active Mount Kaba is a young Mount Kaba in the form of a stratovolcano with a height of 1952 meters above sea level which is in the Mount Kaba area [2], [3]. The character of the eruption of Mount Kaba is an explosive magmatic eruption [4]. In this area there are also several craters and other eruption centers such as monogenetic volcanoes. This indicates the variety of eruption processes that have occurred in the Mount Kaba area [5]. Research on the geochemistry of rocks in the Mount Kaba area is important to understand the dynamic process of magma evolution in the area. The variety of eruption processes that have occurred in the Mount Kaba area raises questions about the dynamics of magma evolution in the research area based on rock geochemical data [6]. The aim of this research is to find out how the dynamic process of magma evolution is related to the formation of volcanoes in the research area [7]. The location of the research area is in the northern part of the Mount Kaba area, Sumber Urip Village, Selupu Rejang District, Kab. Rejang Lebong, Bengkulu Province [8], [9].

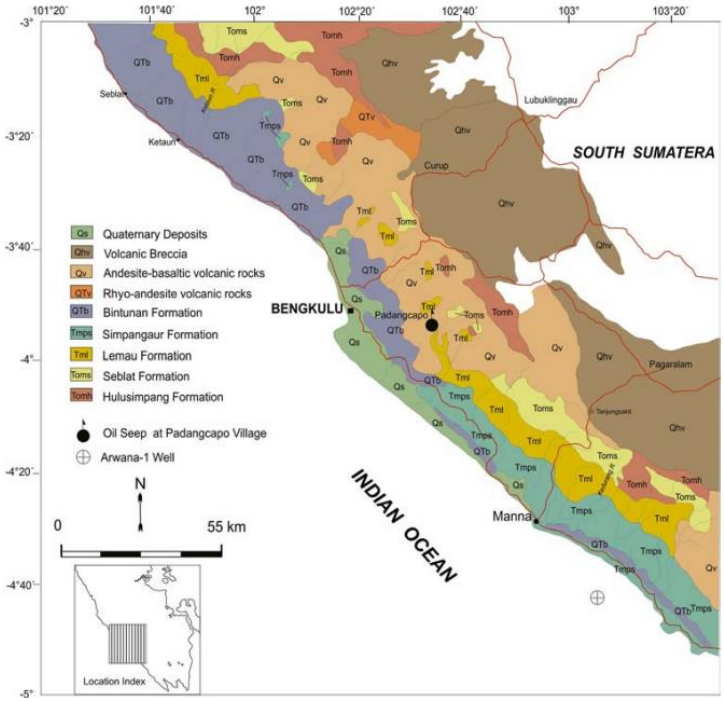

Figure 1. Geological map of Bengkulu sheet [14] modified by [15].

This study was specifically focused on the northern sector of the study area, where all sampling activities were conducted systematically within this region. The selection of the northern sector was based on several volcanological and practical considerations aligned with the objectives of the research [8]. Spatially, the northern area hosts significant population settlements and a distribution of monogenetic volcanoes that are interpreted to have potential genetic and evolutionary relationships with the main volcanic edifice [10]. Accordingly, this study aims to evaluate the magmatic connections between the primary volcanic center and the monogenetic volcanic systems located to the north [11]. In addition, geomorphological data and eruption history indicate a dominant trend of pyroclastic flow emplacement toward the northern sector, highlighting its importance in the context of volcanic hazard mitigation [12]. Therefore, the restriction of the study area to the northern sector represents a deliberate methodological decision, focused on understanding local magmatic system relationships and their implications for volcanic risk assessment in the most vulnerable region [8], [13].

Geology of the Research Area

Based on Figure 1 of the geological map sheet of Bengkulu [14] modified by [15], the research area consists of 1 unit, namely the Volcano Breccia Unit (Qhv), which consists of volcanic breccia, lava, and tuff with andesite-basal composition from Mount Kaba.

2. Methodology

Geochemical analysis aims to determine the types of elements contained in the minerals that make up rocks. In this research, geochemical analysis uses the ICP-MS (Inductively Coupled Plasma Emission Mass Spectrometry) analysis method to determine main elements, trace elements, and rare earth elements [16]. ICP-MS geochemical analysis was performed at the ALS Geochemistry Laboratory of Canada. There are 15 rock samples to be analyzed. To obtain geochemical trends, 3 rock samples were taken from each volcano. The measurement results are processed using software such as Microsoft Excel, and normalization of the geochemical data is carried out [17]. Then use the help of other software, such as Winrock, to plot the data in geochemical diagrams to see the distribution of elements and interpret the data [18]. Data from the analysis of major elements and trace elements will be used as indicators and parameters of petrogenesis to find out about magma characteristics (magma origin), rock types, tectonic environment, petrogenesis models, and identify processes that occur in magma chambers (magma differentiation), which consist of fractional crystallization, assimilation and magma mixing [19].

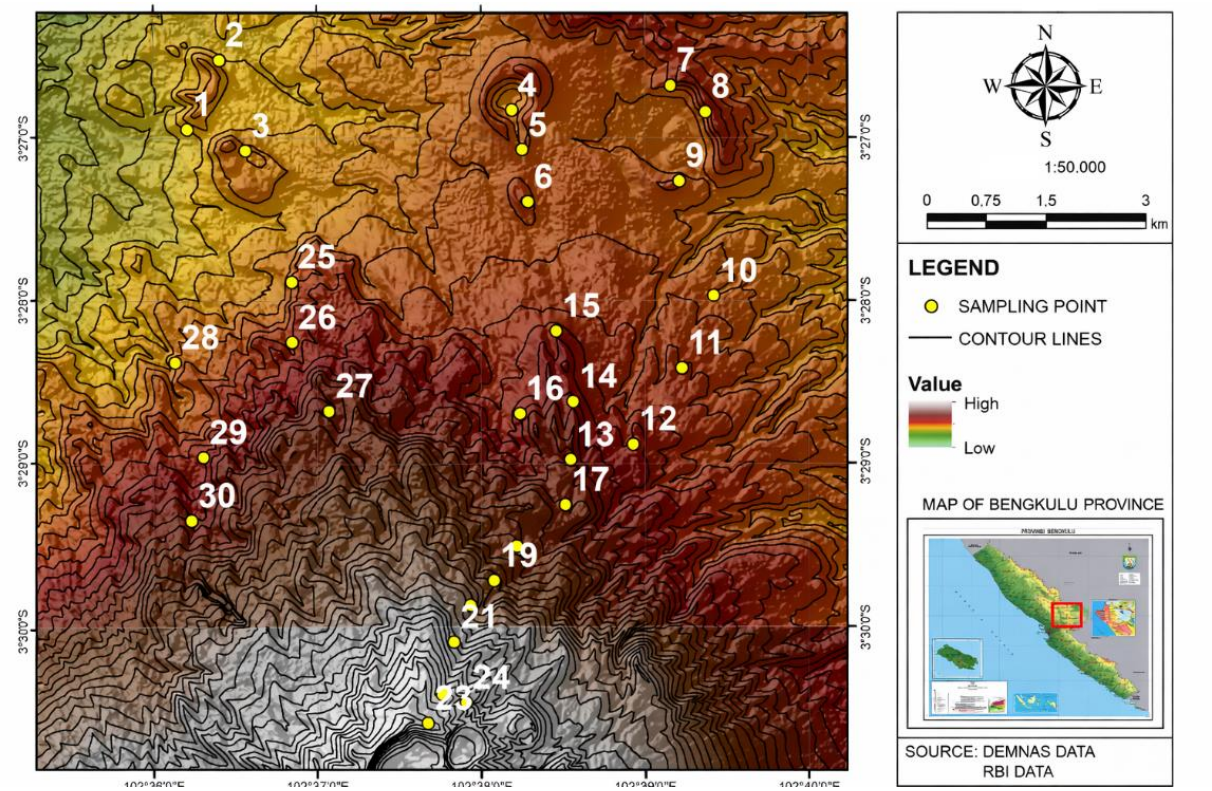

Figure 2. Map of Geochemical Sampling Points in the Research Area.

3. Results and discussions

In Figure 2, the geochemical sampling point map of the research area shows that not all of the sampling points were subjected to geochemical analysis. Geochemical analysis of rocks in the research area was carried out on rock samples representing lithological units. These rock samples include lava samples and pyroclastic rock samples. Data from the geochemical analysis of rocks is attached on the attachment page.

Rock samples in the research area have a LOI value range of 0.11 – 2.36 wt%, indicating that the condition of the samples is still quite fresh even though slightly weathered so that they can produce quite good geochemical data. The LOI value for the sample was normalized so that the LOI content was 0% and the total main elements were 100% [20].

Petrological and Mineralogical Characteristics of Rocks

Based on petrographic analysis, the rocks at the study site are dominated by basalt and andesite, ranging in color from light gray to dark gray. In general, the rocks exhibit a hypocrystalline degree of crystallinity with a porphyritic texture and inequigranular grain uniformity, with crystallite sizes ranging from 0.1–1 mm and euhedral to anhedral crystal forms. Samples STA 1 and STA 4 are classified as vesicular basalt, characterized by a vitrophyric texture, vesicular structure, and high vesicle and glass content. Meanwhile, STA 7 and STA 8 are massive basalts with aphanitic–porphyritic textures and primarily composed of olivine, pyroxene, plagioclase, K-feldspar, and microlite [19], [21], [22].

The other samples (STA 13, STA 17, STA 22, STA 23, STA 27, and STA 29) are classified as andesites, which generally have a massive structure with distinctive textural variations such as subophytic, glomeroporphyritic, poikilitic, and intersertal. The mineral composition of andesites is dominated by plagioclase, pyroxene, and K-feldspar, accompanied by hornblende in some samples, and significant glass and microlite content. Overall, the petrographic characteristics indicate a volcanic igneous rock formed by the relatively rapid cooling of magma, with textural and structural variations reflecting differences in magma freezing conditions and evolution [23], [24].

The lava found in the study area shows a fairly wide variation in SiO_2 content, ranging from 50.89 to 63.41 percent by weight (wt%). This chemical composition indicates that the lava in this region falls within the range of mafic to intermediate to slightly felsic types. The primary mineralogy that makes up the lava consists of olivine, pyroxene, and plagioclase, which are typical minerals in lavas with basaltic to andesitic compositions [25]. Changes in mineralogical composition are closely related to increasing SiO_2 levels, where these minerals undergo transitions or replacements according to magma evolution [26]. At SiO_2 values of around 50.89 wt%, olivine is dominant and becomes the main mineral, but the percentage of olivine gradually decreases as the SiO_2 content increases until it reaches around 59 wt%. Subsequently, pyroxene begins to appear and replaces olivine as the dominant mineral in lava with an SiO_2 content of around 58 wt%. In addition, in lava with a more felsic SiO_2 content, namely around 60 wt%, hornblende minerals begin to be present as part of the mineral assemblage, marking a magma phase that is increasingly developing and contains more water and volatiles [19].

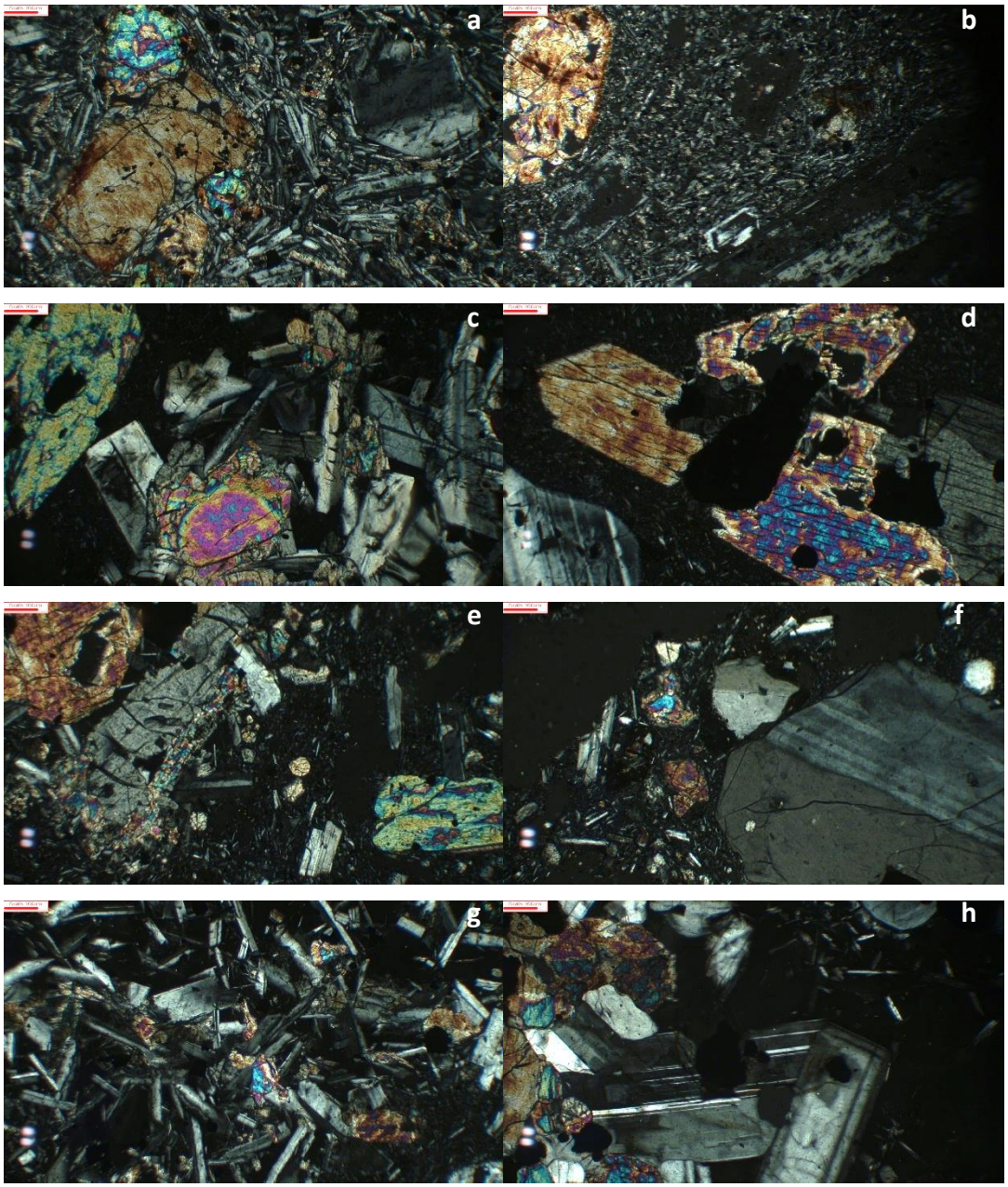

Figure 3. Rock & Mineral Textures Observed from Thin Sections: Trachytic (a), sieve (b), subophytic (c), sieve (d), reaction rim (e), porphyritic (f), intersertal (g), zoning (h).

Several rock textures were found in thin sections in the study area. Among them, porphyritic textures are commonly present in several samples from the study area. This indicates a two-stage magma cooling process [27]. The magma cooling process begins with slow cooling, forming phenocrysts within the magma chamber. This is followed by rapid cooling within the conduit as the magma migrates toward the surface, forming microliths [28], [29]. The closer the magma approaches the surface, the faster the cooling occurs due to the difference in temperature between the magma and the surface [28].

Zoning textures indicate compositional changes during mineral growth. Zoning textures found in plagioclase minerals in thin sections of rocks indicate a change in magma composition to become more andesitic or basaltic [30]. Sieve textures indicate mineral dissolution into melt due to chemical imbalances. These imbalances can occur due to convection within the magma chamber, magma mixing, or the supply of new magma to the already differentiated magma, causing the mineral to be exposed to changes in magma temperature and return to melt [31]. Reaction rim textures are characterized by concentric layers of one mineral enveloping another mineral that formed earlier. This texture indicates a reaction due to chemical imbalances that change the mineral composition at the edges. Figure 3 shows reaction rim textures between minerals, indicating changes in magma composition that trigger mineral changes. These reaction rim textures provide evidence of an open differentiation system within the magma chamber [30].

Geochemical Data: **Rock Types and Magma Affinity**

Determining rock types can be done using main element data such as SiO_2, K_2O, and Na_2O (The fully elements results are attached in the appendix 1). The geochemical data of the main rock elements are plotted into several rock geochemical classification diagrams. This classification is like the classification of rock types based on Total Alkali Silica (TAS) content according to [32] and magma affinity classification based on K_2O according to [33].

Based on Figure 4, the geochemical plot of rocks in the research area on the TAS diagram according to [32], it is known that the geochemical composition of the rocks in the study area consists of andesite, basaltic - andesite, trachyandesite, basanite/tephrite, basalt, and dacite, with SiO_2 values of 44.41-63.41 wt%.

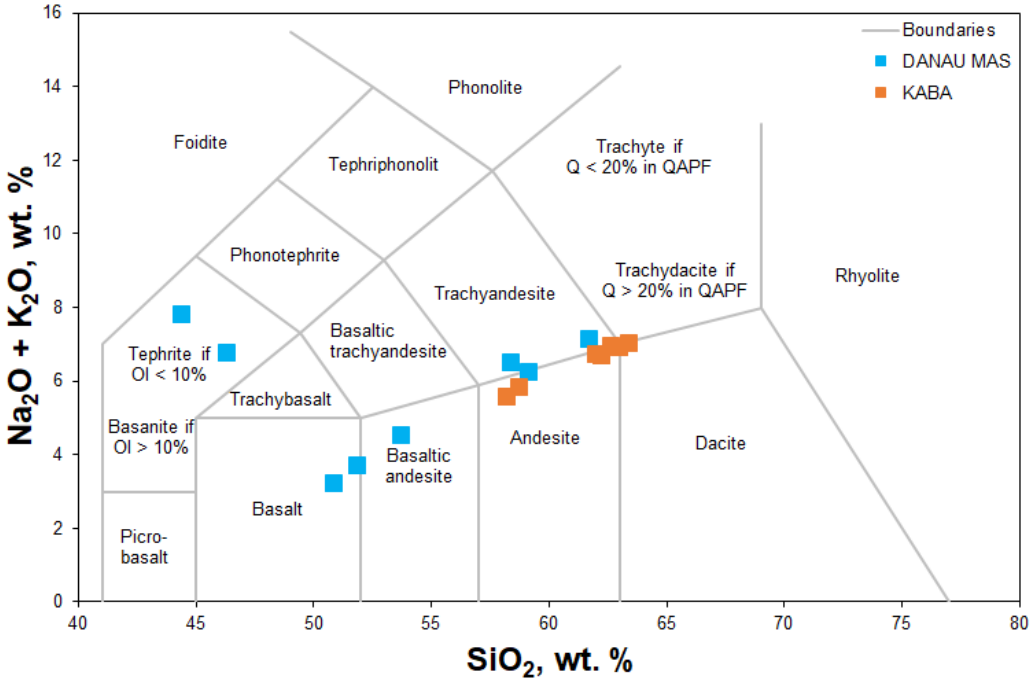

Figure 4. Geochemical plot of rocks in the study area on the TAS diagram according to [32] based on the sample group.

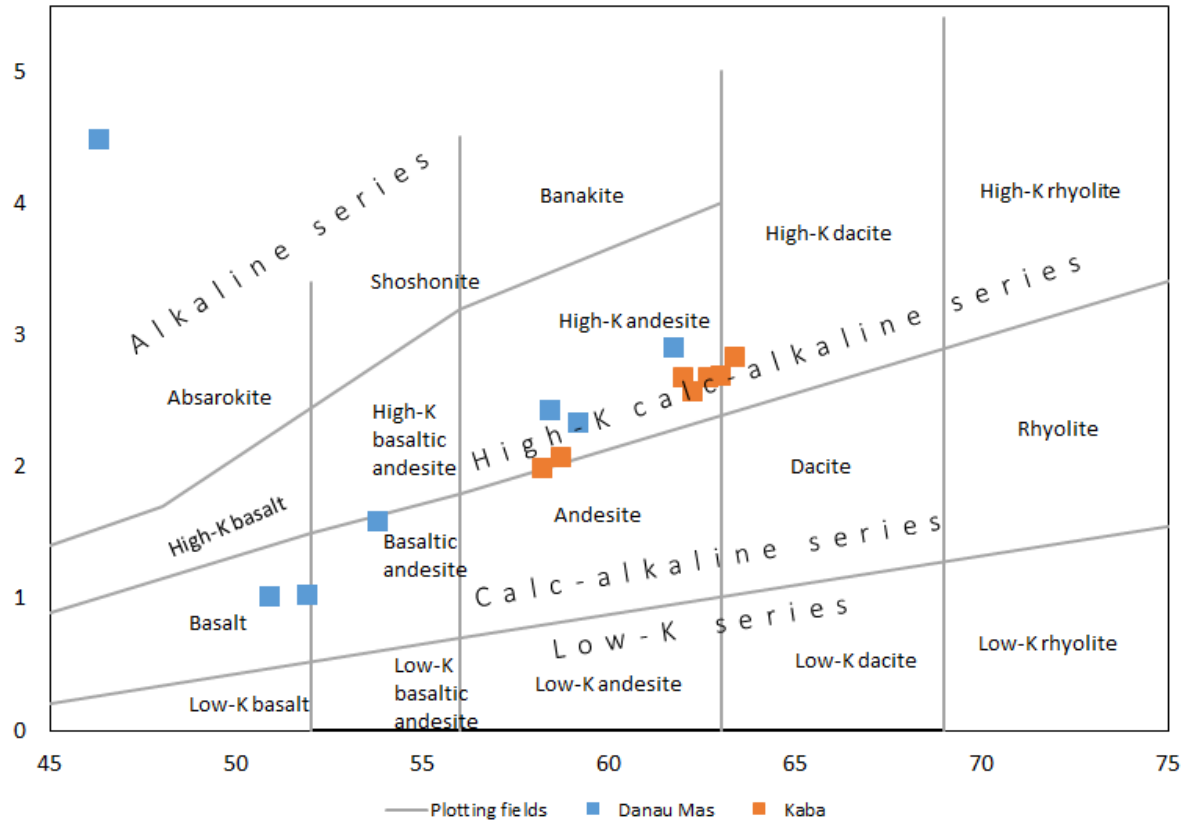

Figure 5. Distribution of magma types in the research area based on the K_2O vs SiO_2 rock geochemical diagram plot [33]

Two samples show the most mafic composition with SiO_2 values of 44.41-46.32 wt% (basanite/tephrite), namely samples 4 and 5. Samples 9, 13, 17, 20, 22, 23, 27, and 29 have SiO_2 values of 58.23-63.41 wt% (andesite-dacite). Meanwhile, samples 1, 2, and 3 are in the SiO_2 value range of 53.79-59.19 wt% (basalt-andesite), and samples 7 and 8 have SiO_2 values of 50.89-51.90 wt% (basalt).

Rock samples in the research area are divided into 2 groups, namely Danau Mas group samples and Kaba group samples. According to Figure 5, division of magma types in the study area based on the K_2O vs SiO_2 rock geochemical diagram plot [33], rock samples 13, 17, 20, 22, 23, 27, and 29 belong to the high-K calc-alkaline magma affinity series (group Kaba). While rock samples 7 and 8 belong to the calc-alkaline series, rock samples 1, 2, 3, and 9 belong to the high-K calc-alkaline series, and rock samples 4 and 5 belong to the alkaline series (Danau Mas group).

The magma in the study area undergoes a differentiation process, which changes the composition of the magma from basaltic to andesitic-dacitic as the SiO_2 content increases [34]. Meanwhile, the presence of basanite/tephrite magma in the alkaline series is characterized by different K_2O+Na_2O contents [35].

Distribution of Main Elements

The distribution of the main elements in the study area is plotted in Figure 6, a Harker diagram plot [36] which depicts the distribution of the main elements (Y axis) against the SiO_2 value (X axis). The SiO_2 value shows the magma differentiation process continuing along with a large increase in value towards the right part of the diagram [37]. The plot of Na_2O and K_2O values shows an increase in values relative to SiO_2 (positive data trend). Meanwhile, the plot of Al_2O_3, CaO, MgO, FeO, MnO, and TiO_2 values shows a decrease in relation to SiO_2 (negative data trend).

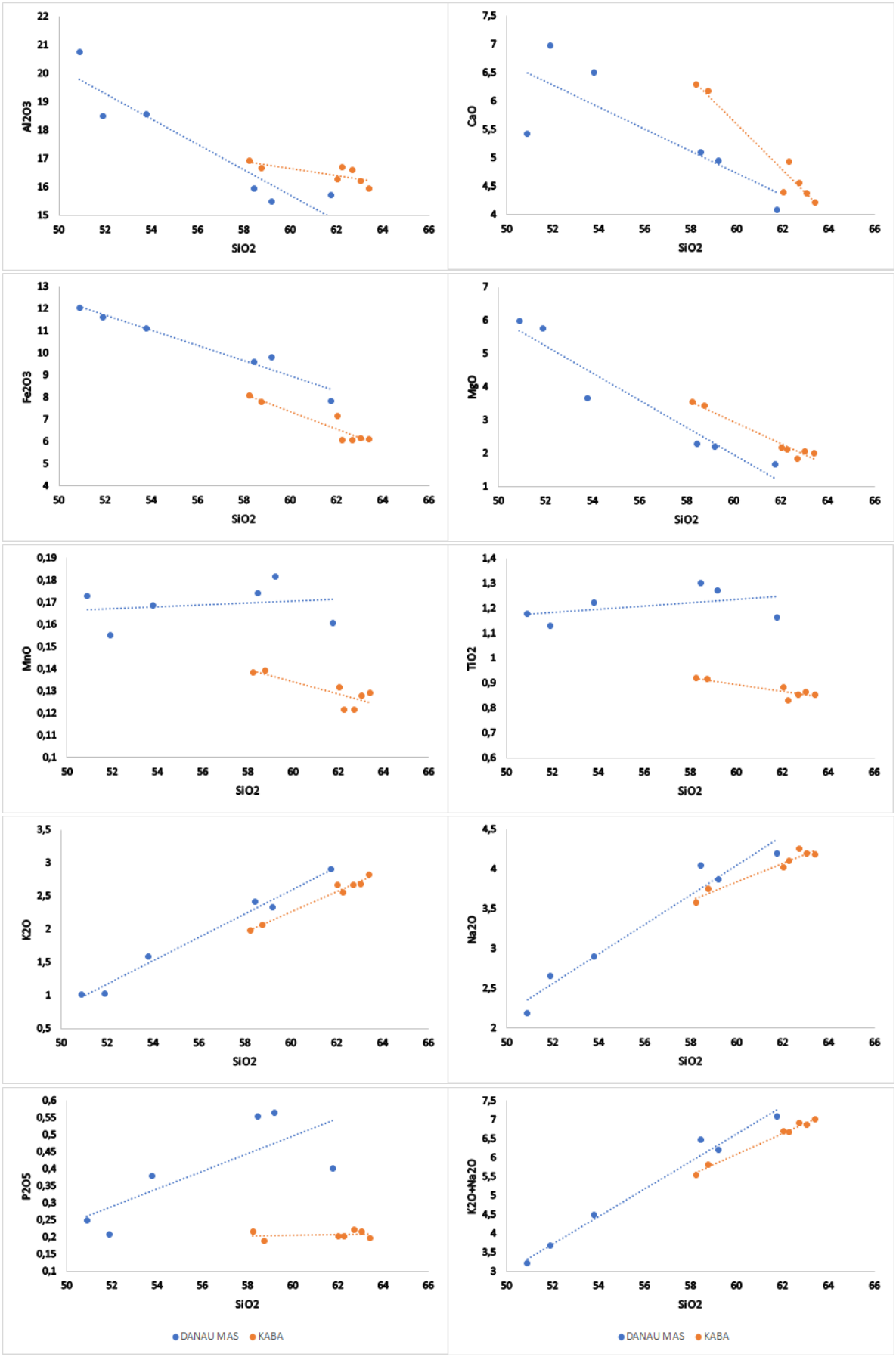

Figure 6. Plot diagram of Harker [36] depicting the distribution of the main elements by magma type, showing a separate trend between type 1 and type 2 magmas in the study area.

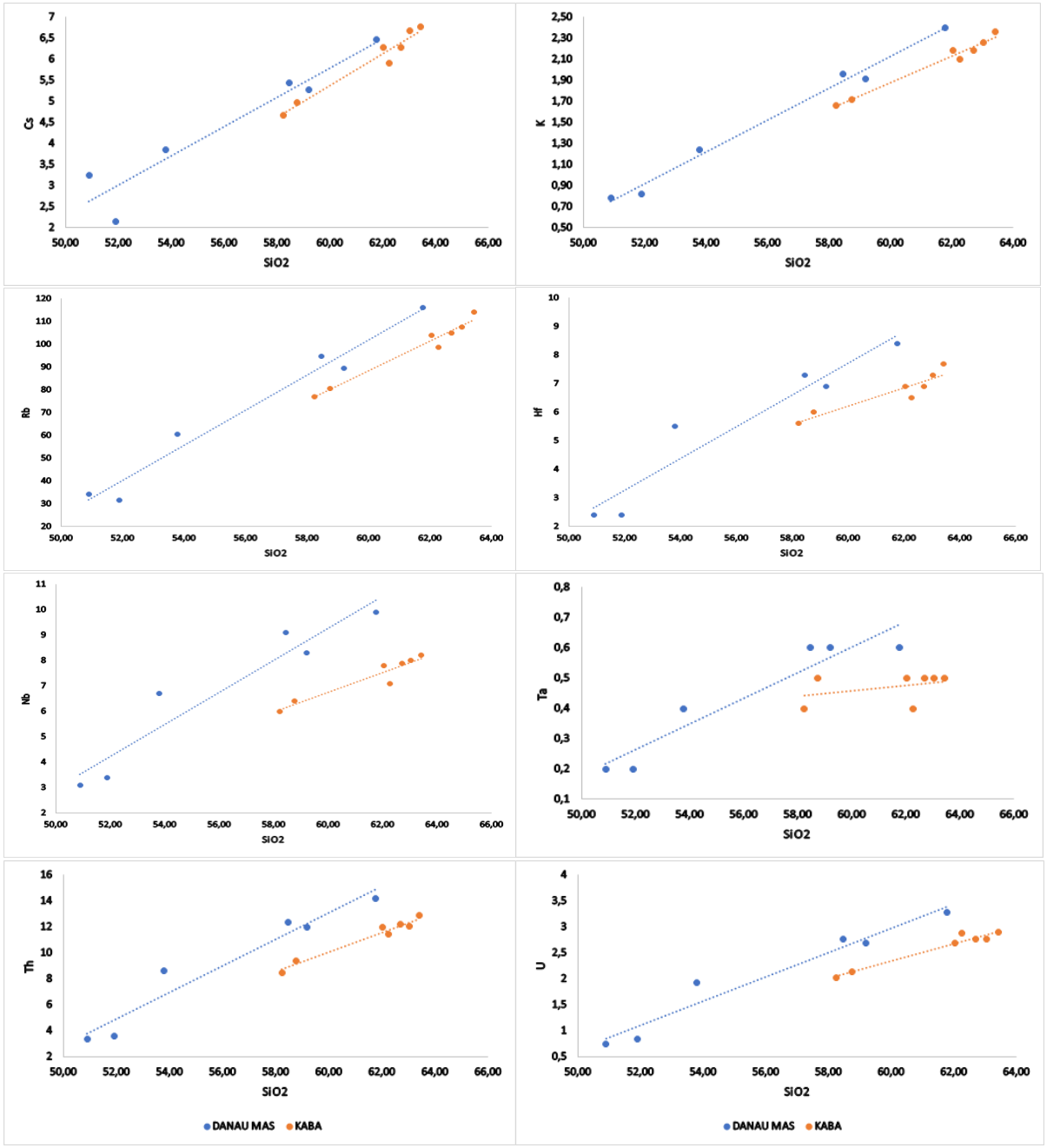

Figure 7. Plot diagram of Harker [36] which depicts the distribution of trace elements based on magma type showing that there is a separate trend between type 1 and type 2 magmas in the study area: Cs (a), K (b), Rb (c), Hf (d), Nb (e), Ta (f), Th (g) and U (h).

Based on the Harker diagram [36], it can be seen that there is a relationship between the location of the rocks in the research area and the level of SiO_2 content in the rocks. Rocks in the southern part of the study area tend to be more felsic with higher NaO_2 and K_2O contents. This is different from the levels of MgO and Fe_2O_3 content for rocks in the northern part of the research area, which tend to be more mafic [8].

Distribution of Trace Elements

The distribution of trace elements in the research area in Figure 7 is a plot of the Harker diagram [36], which depicts the distribution of trace elements based on magma type with SiO_2 values as the X axis and trace elements as the Y axis. The trace elements used include Cs, K, and Rb as representatives of

LILE incompatible elements. Meanwhile, Hf, Nb, Ta, Th, and U are representatives of HFSE incompatible elements. All elements show a positive trend with an increase in SiO_2 [38].

Trace element Harker diagrams show that all LILE (Cs, K, Rb) and HFSE (Hf, Nb, Ta, Th, U) display positive correlations with increasing SiO_2, which geologically reflects the progressive enrichment of incompatible elements during magma evolution [39]. The trend lines on the diagrams explicitly represent magma differentiation pathways primarily controlled by processes such as fractional crystallization, further modified by assimilation and magma mixing [40]. During fractional crystallization, early-formed mafic minerals and plagioclase crystallize and are removed from the melt, causing incompatible elements, those that do not readily enter crystal structures, to become increasingly concentrated in the residual, more silica-rich melt. This enrichment produces the consistent positive linear relationships observed between SiO_2 and trace element concentrations across the diagrams [41].

The behavior of LILE such as Cs, K, and Rb reflects their high mobility and strong tendency to remain in the melt rather than being incorporated into early-forming mafic minerals. Therefore, the systematic increase of LILE with rising SiO_2 indicates progressive evolution toward more differentiated, felsic magma compositions. Meanwhile, HFSE (Hf, Nb, Ta, Th, U) possess high valence and relatively small ionic radii, making them generally incompatible in most common mineral phases. Their increasing concentrations with SiO_2 further support progressive magmatic differentiation, whereby the residual melt becomes enriched in elements not incorporated into early crystals. Variations in the slopes of LILE and HFSE trends may also reflect differences in mineral partition coefficients or the influence of additional processes such as crustal assimilation, which can preferentially enrich certain elements, particularly Th and U [42].

The presence of dual trends in several diagrams suggests that the samples may derive from two distinct magma groups or have undergone different differentiation histories [43]. Differences in the position and slope of trend lines between groups (Danau Mas and Kaba) may indicate variations in magma source characteristics, degrees of differentiation, or episodes of magma mixing that produced chemically distinct magma populations [44]. In addition, assimilation of crustal material during magma evolution may shift incompatible element compositions and generate parallel or subparallel trends on Harker diagrams. Overall, the geochemical patterns indicate that the primary differentiation pathway was governed by fractional crystallization, while assimilation and magma mixing also played significant roles, producing compositional diversity and dual trends that reflect a complex and dynamic magmatic system with repeated thermal and chemical evolution [45].

The pattern of trace elements in the study area in Figure 8 spider diagram of trace elements in the study area normalized to the primitive mantle [46], shows that the magma content is richer in trace elements in the form of enrichment of LILE elements against HFSE elements. The pattern of REE elements in Figure 8 of the REE spider diagram of the research area normalized to chondrite [46], generally shows that the rocks of the research area experience LREE enrichment and HREE depletion.

The influence of SiO_2 values on trace element content is relatively identical to the pattern of REE values. The higher the SiO_2 value, the more enriched the rock is in trace elements, as shown by the pattern of REE values , which tend to increase. The Danau Mas group products with low SiO_2 values can indicate rocks that are poorer in REE elements than the Kaba group products, which have undergone further magma differentiation [47].

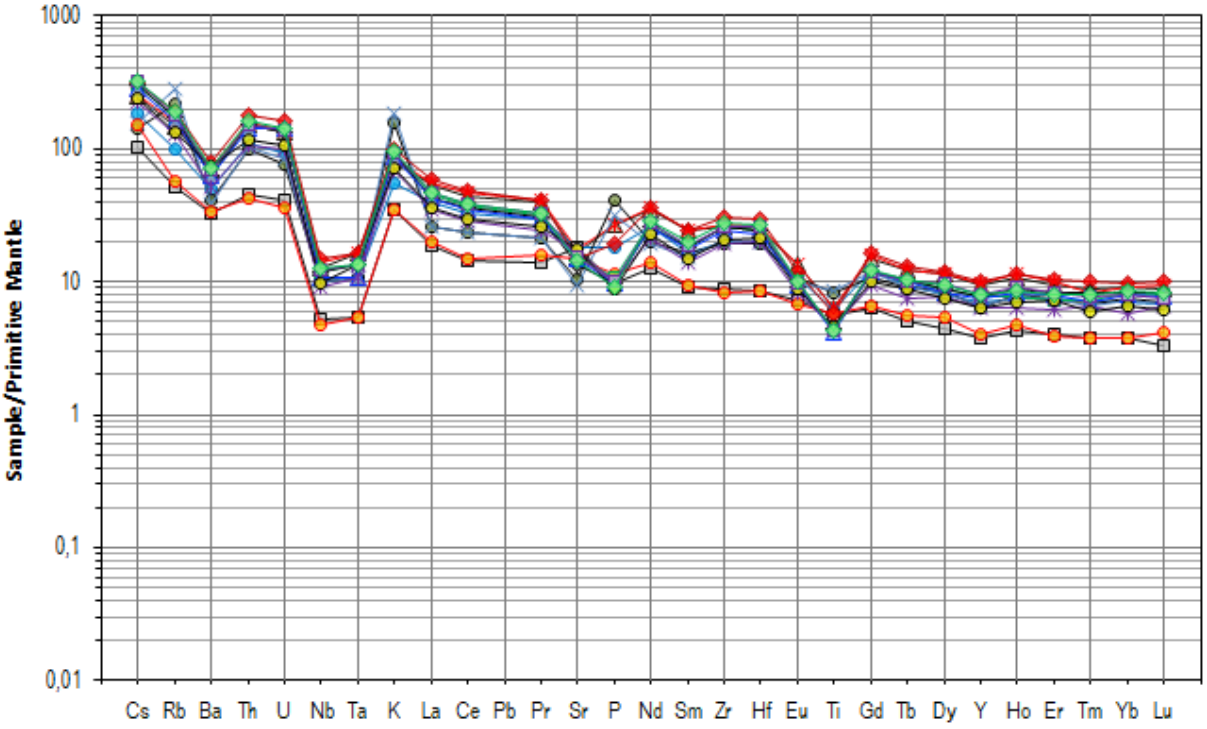

Figure 8. Spider diagram of trace elements in the study area normalized to the primitive mantle [46] based on sample number.

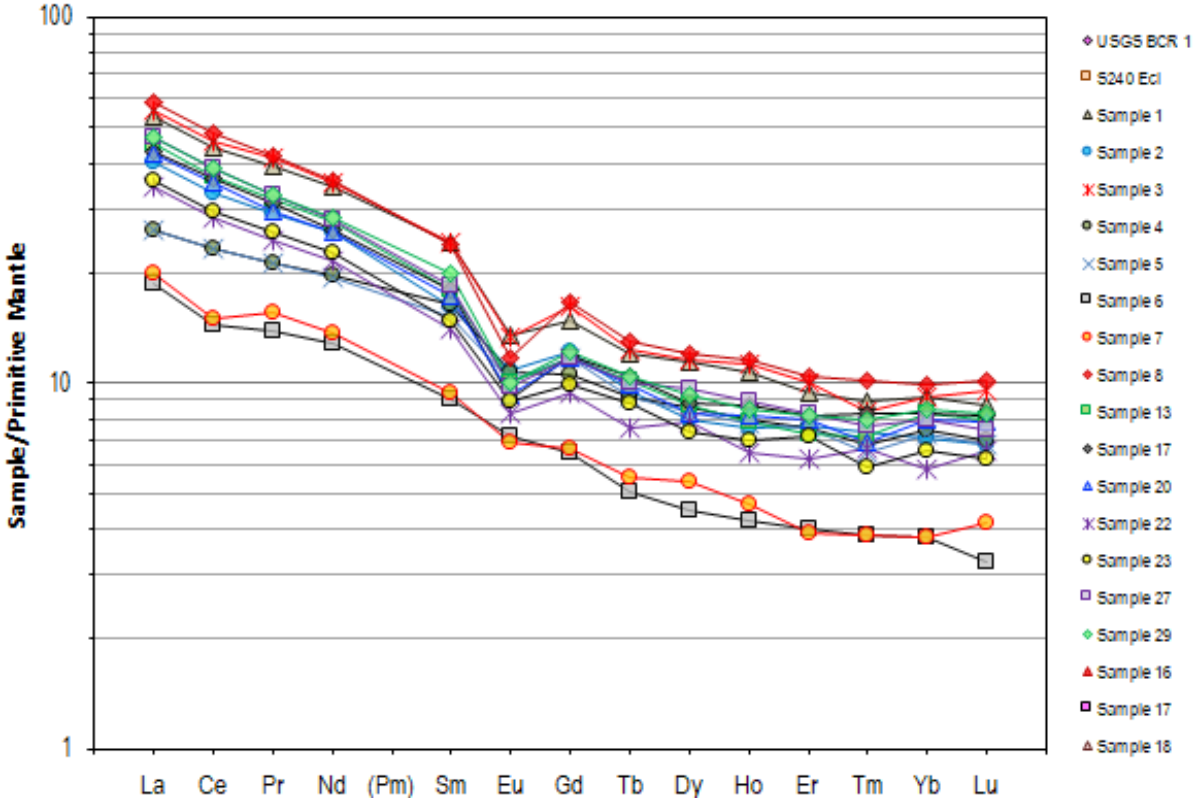

Figure 9. REE spider diagram of the research area normalized to chondrite [46] based on sample number.

Magma type

Magma that undergoes a differentiation process in the same system will be in the same type of magma affinity or geochemical trend. If on 1 volcano there is a separate geochemical data trend, it can be assumed that there is more than one type of magma on that volcano [48]. Geochemical data plots show indications of more than 1 magma affinity trend in the study area. At high-K magma affinity, the trend of K_2O data towards SiO_2 shows a positive gradient. Meanwhile, the trend of K_2O data on calc-alkaline or medium-K affinity is relatively flat.

An overview of the content of main elements and trace elements in the research area can also be seen in the Harker diagram [36], where it can be seen that there is an increasing trend of main elements such as K_2O and Na_2O content along with increasing SiO_2 content. Rocks in the Kaba group have a higher SiO_2 content, while rocks in the Danau Mas group have a different SiO_2 content. Other things can also be seen, such as a decrease in the MgO, CaO, Fe_2O_3, and Al_2O_3 content as the SiO_2 content increases. Harker's plot diagram [36] shows that there are two trends in magma types that experience separate differentiation processes in the study area.

Magma Source

Trace element and REE geochemical data for the study area, normalized to primitive mantle and chondrite, show patterns on the spider diagram. Normalization to the primitive mantle shows a thinning of HFSE relative to LILE (Figure 8). While normalization to chondrite shows an enrichment of LREE over HREE (Figure 9), this pattern of LREE enrichment over HREE, LILE enrichment, and HFSE depletion is a typical characteristic of magmas produced in subduction zones [49].

The LILE element is mobile and is easily carried or fractionated in fluids such as H_2O. The enrichment of these elements in the rocks in the study area is caused by the influence of the addition of fluid to the mantle from the oceanic crust during the plate subduction process [50]. H_2O originating from marine sediments or dehydrated subducting oceanic crust becomes enriched by LILE. This LILE-rich H_2O then lowers the melting point of the mantle and produces subduction zone magmatism [51]. Meanwhile, the HFSE (High Field Strength Element) element is immobile, and its content remains relatively unchanged from the mantle to the surface. So when the HFSE element content in the sample is normalized against the mantle and compared with LILE, it tends to be more prone to depletion [52].

Based on Figure 9, the REE spider diagram of the research area normalized to chondrite [46], it can be seen that there are two patterns. The first pattern shows the enrichment of REE elements. Meanwhile, the second pattern shows less/lower REE content. The patterns of trace elements and REE in the spider diagrams of both magma types are relatively similar, indicating that a magma source from the mantle in both types of magma has the same character. There are magma trends that are slightly richer than other magma trends, although they are not significantly separated. This can be caused by shallow differentiation processes in the crust producing magma that is more evolved and richer in trace elements [19].

Magma Differentiation Process

Magma differentiation in the form of fractional crystallization in the magma of the research area is confirmed by the pattern of the Harker diagram [36], where Al_2O_3, CaO, MgO, FeO, MnO, and TiO_2 decrease as SiO_2 increases, while Na_2O and K_2O pattern increases as SiO_2 increases. In the Harker diagram of trace elements (Figure 7), compatible elements decrease along with magma differentiation because they are bound in a crystal system. Meanwhile, incompatible elements increase with magma differentiation because incompatible elements do not combine with the crystal system and are concentrated in the residual melt [53], [54].

Based on the combination of petrographic and geochemical data, the magma evolution likely involved fractional crystallization as the primary process, accompanied by indications of assimilation and magma mixing as secondary processes that modified the melt composition [55]. Harker diagram trends showing decreasing FeO, MgO, and CaO with increasing SiO_2 indicate the fractionation of mafic minerals such as olivine, pyroxene, and plagioclase during the early stages of differentiation. Conversely, the increase of Na_2O with SiO_2 reflects enrichment in sodium-rich feldspar phases and the evolution toward more felsic magma compositions [56].

From a petrographic perspective, the presence of porphyritic and intersertal textures suggests a two-stage cooling history, early crystallization at depth followed by more rapid solidification at shallower levels, typical of evolving magmatic systems. Trachytic texture indicates viscous, feldspar-rich magma flow during the later stages of crystallization [57]. The occurrence of sieve texture and zoning in plagioclase crystals reflects chemical disequilibrium and rapid changes in physicochemical conditions, commonly associated with magma mixing or compositional changes caused by new magma injections [58]. Meanwhile, reaction rims and subophitic textures indicate mineral melt reactions related to changes in melt composition, which may be interpreted as evidence of assimilation of wall rock material or interaction between magmas of different compositions [59].

Overall, the data suggest that the parental magma underwent significant differentiation through fractional crystallization, producing systematic major and trace element trends [60]. During this evolution, injections of new magma likely triggered magma mixing, as reflected by disequilibrium textures such as sieve texture and zoning [61]. In addition, interaction between magma and surrounding country rock (assimilation) further modified the melt composition and produced reaction textures such as reaction rims [62]. The combination of these three processes, dominant fractional crystallization, accompanied by assimilation and magma mixing, indicates a dynamic magmatic system characterized by repeated thermal and chemical changes throughout its evolutionary history [63].

4. Conclusion

This study of the northern sector of Mount Kaba reveals basaltic-andesitic volcanic rocks formed within a complex subduction-related magmatic system. Petrographic textures and ICP-MS geochemical data indicate two magma groups (Danau Mas and Kaba) with calc-alkaline to high-K affinities and compositions ranging from basanite/tephrite to dacite. Major and trace element Harker diagrams, REE and spider patterns show LILE enrichment, HFSE depletion, and LREE-enriched signatures, reflecting mantle-derived magma modified in the crust. Magma evolution was dominated by fractional crystallization, accompanied by assimilation and magma mixing, producing dual geochemical trends and compositional diversity. These findings clarify magmatic connections with northern monogenetic volcanoes and provide insight for volcanic hazard assessment.

Acknowledgment

The author would like to express his gratitude to the Petrology Laboratory of Institut Teknologi Sumatera for their support during the research process.

References:

[1] Permana, S., Lubis, D. P., Marbun, S. F., & Amelia, P. (2025). The Meaning of Place in Historic Building (Case Study: Three Urban Heritage Tourism Destinations at Kesawan Medan). *Jurnal Penelitian Geografi*, *13*(2), 223-242.

[2] Natawidjaja, D. H. (2003). Neotectonics of the Sumatran Fault and paleogeodesy of the Sumatran subduction zone. California Institute of Technology.

[3] Sieh, K., & Natawidjaja, D. (2000). Neotectonics of the Sumatran fault, Indonesia. *Journal of Geophysical Research: Solid Earth*, *105*(B12), 28295-28326.

[4] Sugianto, N., Nukman, M., & Suryanto, W. (2023). Characteristics of Active Volcanoes in Sumatra, Indonesia: From Perspective Seismicity, Magma Chemical Composition and Eruption History. In *E3S Web of Conferences* (Vol. 468, p. 09002). EDP Sciences.
[5] Kusumadinata, K., Hadian, R., Hamidi, S. and Reksowirogo, L.D., 1979. Data dasar gunungapi Indonesia. *Direktorat Vulkanologi, Bandung*, *820*.
[6] Mibei, G., Bali, E., Geirsson, H., Guðfinnsson, G. H., Harðarson, B. S., & Franzson, H. (2021). Partial melt generation and evolution of magma reservoir conditions at the Paka volcanic complex in Kenya: Constraints from geochemistry, petrology and geophysics. *Lithos*, *400*, 106385.
[7] Sparks, R. S. J., & Cashman, K. V. (2017). Dynamic magma systems: Implications for forecasting volcanic activity. *Elements*, *13*(1), 35-40.
[8] Wijaya, M. E. J., & Setijadji, L. D. (2022). A Preliminary Volcanological Study of North Eastern Kaba Volcano, Bengkulu Province, Indonesia. IOP Conference Series: Earth and Environmental Science (Vol. 1071, No. 1, p. 012018). IOP Publishing.
[9] Wijaya, M. E. J., & Mentari, S. G. (2025). Karakteristik Geokimia Batuan Unsur Jejak dan Unsur Tanah Jarang Gunung Api Kaba untuk Interpretasi Tatanan Tektonik Berdasarkan Analisis ICP-MS. *Jurnal Penelitian Inovatif*, *5*(3), 2311-2320.
[10] Németh, K., & Kereszturi, G. (2015). Monogenetic volcanism: personal views and discussion. International Journal of Earth Sciences, 104(8), 2131-2146.
[11] Murcia, H., Borrero, C., & Németh, K. (2019). Overview and plumbing system implications of monogenetic volcanism in the northernmost Andes' volcanic province. Journal of Volcanology and Geothermal Research, 383, 77-87.
[12] Manville, V., Newton, E. H., & White, J. D. (2005). Fluvial responses to volcanism: resedimentation of the 1800a Taupo ignimbrite eruption in the Rangitaiki River catchment, North Island, New Zealand. Geomorphology, 65(1-2), 49-70.
[13] Favereau, M., Robledo, L. F., & Bull, M. T. (2018). Analysis of risk assessment factors of individuals in volcanic hazards: Review of the last decade. Journal of Volcanology and Geothermal Research, 365, 57-64.
[14] Gafoer, S., Amin, T.C. and R.. Pardede, 1992. Peta geologi lembar Bengkulu, Sumatra. Pusat Penelitian dan Pengembangan Geologi.
[15] Panggabean, H., & Heryanto, R. (2009). An appraisal for the petroleum source rocks on oil seep and rock samples of the Tertiary Seblat and Lemau Formations, Bengkulu Basin. *Indonesian Journal on Geoscience*, *4*(1), 43-55.
[16] Rollinson, H. R. (1993). Using geochemical data: evaluation, presentation, interpretation. Routledge.
[17] Zhou, J., & Li, X. (2006). GeoPlot: An Excel VBA program for geochemical data plotting. *Computers & Geosciences*, *32*(4), 554-560.
[18] Janoušek, V., Farrow, C. M., & Erban, V. (2006). Interpretation of whole-rock geochemical data in igneous geochemistry: introducing Geochemical Data Toolkit (GCDkit). *Journal of Petrology*, *47*(6), 1255-1259.
[19] Winter, J. D. (2014). *Principles of igneous and metamorphic petrology* (Vol. 2). Harlow, UK: Pearson education.
[20] Le Maitre, R. W., Streckeisen, A., Zanettin, B., Le Bas, M. J., Bonin, B., & Bateman, P. (Eds.). (2005). *Igneous rocks: a classification and glossary of terms: recommendations of the International Union of Geological Sciences Subcommission on the Systematics of Igneous Rocks*. Cambridge University Press.
[21] Best, M. G. (2002). *Igneous and metamorphic petrology*. John Wiley & Sons.
[22] Philpotts, A. R., & Ague, J. J. (2009). *Principles of igneous and metamorphic petrology*. Cambridge University Press.
[23] Jerram, D. A., Dobson, K. J., Morgan, D. J., & Pankhurst, M. J. (2018). The petrogenesis of magmatic systems: Using igneous textures to understand magmatic processes. In *Volcanic and igneous plumbing systems* (pp. 191-229). Elsevier.
[24] Gill, R., & Fitton, G. (2022). *Igneous rocks and processes: a practical guide*. John Wiley & Sons.
[25] Dietrich, V. J., & Popa, R. G. (2017). Petrology and geochemistry of lavas and pyroclastics. In *Nisyros Volcano: The Kos-Yali-Nisyros Volcanic Field* (pp. 103-144). Cham: Springer International Publishing.

[26] Putnis, A. (2009). Mineral replacement reactions. *Reviews in mineralogy and geochemistry*, *70*(1), 87-124.
[27] Yang, Z. F. (2012). Combining quantitative textural and geochemical studies to understand the solidification processes of a granite porphyry: Shanggusi, East Qinling, China. Journal of Petrology, 53(9), 1807-1835.
[28] Marsh, B. D., & Watts, A. B. (2007). Magmatism, magma, and magma chambers. *Treatise on Geophysics: Crust and Lithosphere Dynamics; Watts, AB, Ed*, 275-333.
[29] Caceres, F., Scheu, B., Colombier, M., Hess, K. U., Feisel, Y., Ruthensteiner, B., & Dingwell, D. B. (2022). The roles of microlites and phenocrysts during degassing of silicic magma. *Earth and Planetary Science Letters*, *577*, 117264.
[30] Streck, M. J. (2008). Mineral textures and zoning as evidence for open system processes. *Reviews in Mineralogy and Geochemistry*, *69*(1), 595-622.
[31] Stewart, M. L., & Pearce, T. H. (2004). Sieve-textured plagioclase in dacitic magma: Interference imaging results. *American Mineralogist*, *89*(2-3), 348-351.
[32] Bas, M. L., Maitre, R. L., Streckeisen, A., Zanettin, B., & IUGS Subcommission on the Systematics of Igneous Rocks. (1986). A chemical classification of volcanic rocks based on the total alkali-silica diagram. *Journal of petrology*, *27*(3), 745-750.
[33] Ewart, A. (1982). The Mineralogy and petrology of Tertiary-Recent orogenic volcanic rocks; with special reference to the andesitic-basaltic compositional range. *Andesites: orogenic andesites and related rocks*, 26-87.
[34] Parat, F., Streck, M. J., Holtz, F., & Almeev, R. (2014). Experimental study into the petrogenesis of crystal-rich basaltic to andesitic magmas at Arenal volcano. *Contributions to Mineralogy and Petrology*, *168*(2), 1040.
[35] Brenna, M., Ubide, T., Nichols, A. R., Mollo, S., & Pontesilli, A. (2021). Anatomy of intraplate monogenetic alkaline basaltic magmatism: clues from magma, crystals, and glass. *Crustal Magmatic System Evolution: Anatomy, Architecture, and Physico-Chemical Processes*, 79-103.
[36] Harker, A. (1909). *The natural history of igneous rocks*. Methuen & Company.
[37] Jagoutz, O., & Klein, B. (2018). On the importance of crystallization-differentiation for the generation of SiO2-rich melts and the compositional build-up of arc (and continental) crust. *American Journal of Science*, *318*(1), 29-63.
[38] Jamali, H. (2017). The behavior of rare-earth elements, zirconium and hafnium during magma evolution and their application in determining mineralized magmatic suites in subduction zones: constraints from the Cenozoic belts of Iran. *Ore Geology Reviews*, *81*, 270-279.
[39] Xiao, Y., Niu, Y., Wang, K. L., Lee, D. C., & Iizuka, Y. (2016). Geochemical behaviours of chemical elements during subduction-zone metamorphism and geodynamic significance. International Geology Review, 58(10), 1253-1277.
[40] Zellmer, G. F., Annen, C., Charlier, B. L. A., George, R. M. M., Turner, S. P., & Hawkesworth, C. J. (2005). Magma evolution and ascent at volcanic arcs: constraining petrogenetic processes through rates and chronologies. Journal of Volcanology and Geothermal Research, 140(1-3), 171-191.
[41] Guo, Q., Shields, G. A., Liu, C., Strauss, H., Zhu, M., Pi, D., ... & Yang, X. (2007). Trace element chemostratigraphy of two Ediacaran–Cambrian successions in South China: implications for organosedimentary metal enrichment and silicification in the early Cambrian. Palaeogeography, Palaeoclimatology, Palaeoecology, 254(1-2), 194-216.
[42] Kottke-Levin, J., Tredoux, M., & Gräbe, P. J. (2009). An investigation of the geochemistry of the Middle Group of the eastern Bushveld complex, South Africa Part 1–the chromitite layers. Applied Earth Science, 118(3-4), 111-130.
[43] Zellmer, G. F., Annen, C., Charlier, B. L. A., George, R. M. M., Turner, S. P., & Hawkesworth, C. J. (2005). Magma evolution and ascent at volcanic arcs: constraining petrogenetic processes through rates and chronologies. Journal of Volcanology and Geothermal Research, 140(1-3), 171-191.
[44] Scheu, B., & Dingwell, D. B. (2022). Magma fragmentation. Reviews in mineralogy and geochemistry, 87(1), 767-800.
[45] Lissenberg, C. J., & MacLeod, C. J. (2016). A reactive porous flow control on mid-ocean ridge magmatic evolution. *Journal of Petrology*, *57*(11-12), 2195-2220.

[46] McDonough, W. F., & Sun, S. S. (1995). The composition of the Earth. Chemical geology, 120(3-4), 223-253.
[47] Vural, A. (2020). Investigation of the relationship between rare earth elements, trace elements, and major oxides in soil geochemistry. *Environmental Monitoring and Assessment*, *192*(2), 124.
[48] Perugini, D., & Poli, G. (2012). The mixing of magmas in plutonic and volcanic environments: analogies and differences. *Lithos*, *153*, 261-277.
[49] Kirchenbaur, M., Schuth, S., Barth, A. R., Luguet, A., König, S., Idrus, A., ... & Münker, C. (2022). Sub-arc mantle enrichment in the Sunda rear-arc inferred from HFSE systematics in high-K lavas from Java. *Contributions to Mineralogy and Petrology*, *177*(1), 8.
[50] Fyfe, W. S. (2012). *Fluids in the earth's crust: Their significance in metamorphic, tectonic and chemical transport process* (Vol. 1). Elsevier.
[51] Peccerillo, A., & Frezzotti, M. L. (2015). Magmatism, mantle evolution and geodynamics at the converging plate margins of Italy. Journal of the Geological Society, 172(4), 407-427.
[52] Münker, C., Wörner, G., Yogodzinski, G., & Churikova, T. (2004). Behaviour of high field strength elements in subduction zones: constraints from Kamchatka–Aleutian arc lavas. *Earth and Planetary Science Letters*, *224*(3-4), 275-293.
[53] Kent, A. J. (2008). Melt inclusions in basaltic and related volcanic rocks. *Reviews in mineralogy and geochemistry*, *69*(1), 273-331.
[54] Kumar, S. (2014). Magmatic processes: review of some concepts and models. *Modelling of magmatic and allied processes*, 1-22
[55] Li, C., Niu, M., Yuan, X., Yan, Z., Wu, Q., Li, X., & Sun, Y. (2022). Geochemical signals of coexisting magma mixing and fractional crystallization processes in the arc setting: Case study of Wulan intrusive suite in the NE Tibet Plateau. *Lithos*, *432*, 106914.
[56] Ghaffari, M., Rashidnejad-Omran, N., Dabiri, R., Chen, B., & Santos, J. F. (2013). Mafic–intermediate plutonic rocks of the Salmas area, northwestern Iran: their source and petrogenesis significance. *International Geology Review*, *55*(16), 2016-2029.
[57] Yang, Z. F. (2012). Combining quantitative textural and geochemical studies to understand the solidification processes of a granite porphyry: Shanggusi, East Qinling, China. *Journal of Petrology*, *53*(9), 1807-1835.
[58] Shcherbakov, V. D., Plechov, P. Y., Izbekov, P. E., & Shipman, J. S. (2011). Plagioclase zoning as an indicator of magma processes at Bezymianny Volcano, Kamchatka. *Contributions to Mineralogy and Petrology*, *162*(1), 83-99.
[59] Larrea, P., Galé, C., Ubide, T., Widom, E., Lago, M., & França, Z. (2014). Magmatic evolution of graciosa (Azores, Portugal). *Journal of Petrology*, *55*(11), 2125-2154.
[60] Yan, L. L., He, Z. Y., Klemd, R., Beier, C., & Xu, X. S. (2020). Tracking crystal-melt segregation and magma recharge using zircon trace element data. *Chemical Geology*, *542*, 119596.
[61] Streck, M. J. (2008). Mineral textures and zoning as evidence for open system processes. *Reviews in Mineralogy and Geochemistry*, *69*(1), 595-622.
[62] Browne, B. L., & Gardner, J. E. (2006). The influence of magma ascent path on the texture, mineralogy, and formation of hornblende reaction rims. *Earth and Planetary Science Letters*, *246*(3-4), 161-176.
[63] Spera, F. J., & Bohrson, W. A. (2004). Open-system magma chamber evolution: an energy-constrained geochemical model incorporating the effects of concurrent eruption, recharge, variable assimilation and fractional crystallization (EC-E′ RAχFC). *Journal of Petrology*, *45*(12), 2459-2480.

Appendix 1.

Table of Major Elements, Trace Elements in percent unit (%) in the Study Area

Location	SiO_2	Al_2O_3	Fe_2O_3	CaO	MgO	Na_2O	K_2O	Cr_2O_3	TiO_2	MnO	P_2O_5	SrO	BaO	TOTAL
STA01	59.19	15.50	9.81	4.94	2.21	3.86	2.33	0.0020	1.27	0.18	0.56	0.040	0.050	100
STA02	53.79	18.56	11.12	6.50	3.65	2.90	1.58	0.0074	1.22	0.16	0.37	0.042	0.042	100
STA03	58.45	15.94	9.61	5.09	2.28	4.05	2.42	0.0031	1.30	0.17	0.55	0.041	0.051	100
STA04	46.32	21.19	13.08	5.71	4.17	2.25	4.47	0.0052	1.66	0.20	0.84	0.020	0.031	100
STA05	44.41	21.55	13.88	5.54	4.21	2.44	5.33	0.0040	1.69	0.22	0.65	0.020	0.030	100
STA07	51.90	18.49	11.60	6.98	5.77	2.65	1.02	0.0155	1.12	0.15	0.20	0.041	0.020	100
STA08	50.89	20.74	12.04	5.42	5.99	2.19	1.01	0.0130	1.17	0.17	0.24	0.043	0.021	100
STA09	61.77	15.71	7.84	4.08	1.66	4.19	2.90	0.0020	1.16	0.16	0.40	0.030	0.050	100
STA13	62.70	16.59	6.08	4.56	1.83	4.25	2.66	0.0020	0.85	0.12	0.22	0.040	0.050	100
STA17	62.03	16.26	7.14	4.38	2.17	4.02	2.66	0.0030	0.88	0.13	0.20	0.030	0.040	100
STA20	62.26	16.70	6.07	4.93	2.11	4.11	2.56	0.0020	0.83	0.12	0.20	0.040	0.040	100
STA22	58.23	16.93	8.07	6.29	3.53	3.57	1.98	0.0050	0.92	0.13	0.21	0.039	0.039	100
STA23	58.75	16.67	7.79	6.18	3.42	3.75	2.06	0.0060	0.91	0.13	0.18	0.039	0.049	100
STA27	63.03	16.20	6.14	4.38	2.05	4.19	2.67	0.0020	0.86	0.12	0.21	0.039	0.049	100
STA29	63.41	15.95	6.12	4.21	2.01	4.18	2.82	0.0020	0.85	0.12	0.19	0.029	0.049	100

Table of Transition Metal Elements, Alkali Elements, and Rare Earth Elements in parts per million unit (ppm) in the Study Area

Sample	Ba	Ce	Cr	Cs	Dy	Er	Eu	Ga	Gd	Hf	Ho	La	Lu	Nb	Nd	Pr	Rb	Sm	Sn	Sr	Ta	Tb	Th	Tm	U	V	W	Y	Yb	Zr
STA01	456	74.1	20	5.28	7.67	4.11	2.08	20	8.08	6.9	1.59	34.9	0.59	8.3	43.1	10	89.4	9.9	3	329	0.6	1.2	12	0.61	2.68	112	2	39.9	4.04	269
STA02	335	55.2	50	3.84	5.39	3.33	1.67	21.3	6.65	5.5	1.13	26.1	0.46	6.7	32.6	7.43	60.6	6.62	3	357	0.4	0.94	8.58	0.5	1.92	210	1	30.6	3.14	207
STA03	475	77.2	10	5.45	7.77	4.39	2.05	22.3	8.79	7.3	1.69	35.9	0.64	9.1	44.5	10.5	94.6	9.82	5	351	0.6	1.22	12.35	0.57	2.76	126	2	42.2	4.07	281
STA04	269	39	30	2.96	5.78	3.31	1.65	26.2	5.75	5.5	1.19	17	0.47	6.6	24.7	5.42	130.5	6.72	3	209	0.4	0.91	7.97	0.46	1.56	366	1	27.6	3.29	200
STA05	252	39	30	3.35	5.64	3.31	1.56	25.2	6.35	5.7	1.15	17	0.46	6.6	24.3	5.44	167.5	6.19	4	187.5	0.4	0.91	8.08	0.44	1.69	374	1	28.6	3.19	218
STA07	217	24.2	110	2.14	3.03	1.75	1.11	20.9	3.51	2.4	0.63	12.2	0.22	3.4	16	3.54	31.5	3.66	1	355	0.2	0.5	3.56	0.26	0.84	284	1	16.2	1.68	94
STA08	221	25.1	90	3.24	3.61	1.71	1.06	19.7	3.63	2.4	0.7	13	0.28	3.1	17.2	3.98	34.2	3.83	1	301	0.2	0.55	3.33	0.26	0.74	261	1	17.1	1.67	88
STA09	519	80.9	<10	6.46	8.11	4.6	1.81	21.8	9.01	8.4	1.72	38.2	0.69	9.9	44.9	10.6	116	9.73	4	297	0.6	1.29	14.2	0.69	3.28	70	2	43	4.36	323
STA13	441	61.4	10	6.27	5.87	3.2	1.54	20.2	6.38	6.9	1.17	29.3	0.54	7.9	34.4	8.14	105	7.36	3	307	0.5	1.01	12.2	0.49	2.77	114	2	33.2	3.64	271
STA17	418	60.9	20	6.29	5.92	3.57	1.39	20.2	6.5	6.9	1.3	27.9	0.55	7.8	32.7	7.9	104	7.34	3	273	0.5	1.04	11.95	0.56	2.69	133	2	33	3.64	273
STA20	421	59.1	10	5.91	5.59	3.48	1.44	20	6.35	6.5	1.22	27.6	0.53	7.1	32.3	7.51	98.6	7.01	3	300	0.4	0.98	11.45	0.47	2.88	128	2	32.2	3.51	256
STA22	343	47.8	30	4.67	5.28	2.72	1.28	19.9	5.09	5.6	0.96	22.3	0.44	6	27.1	6.25	77	5.74	2	339	0.4	0.75	8.46	0.45	2.02	185	2	27.6	2.58	204
STA23	487	49.6	40	4.97	4.97	3.13	1.38	20.7	5.41	6	1.04	23.3	0.42	6.4	28.3	6.55	80.6	6.03	3	345	0.5	0.87	9.36	0.4	2.13	177	2	27.6	2.88	216
STA27	456	65	10	6.68	6.54	3.6	1.5	20.2	6.36	7.3	1.34	30.5	0.5	8	35.1	8.3	107.5	7.51	3	311	0.5	1	12.05	0.52	2.76	107	2	34.2	3.49	277
STA29	466	64.8	10	6.76	6.25	3.56	1.54	20.3	6.68	7.7	1.27	30.5	0.56	8.2	35.4	8.35	114	8.09	3	284	0.5	1.03	12.85	0.54	2.89	113	2	34.8	3.76	290